nature materials

SUPPLEMENTARY INFORMATION

DOI: 10.1038/NMAT4155

Coexistence of superconductivity and antiferromagnetism in $(Li_{0.8}Fe_{0.2})OHFeSe$

X. F. Lu[1,2], N. Z. Wang[1,2], H. Wu[3,7], Y. P. Wu[1,2], D. Zhao[1,2], X. Z. Zeng[1,2], X. G. Luo[1,2,8], T. Wu[1,2,8],W. Bao[4], G. H. Zhang[5,6], F. Q. Huang[5,6], Q. Z. Huang[3],and X. H. Chen[1,2,8]

1. Hefei National Laboratory for Physical Sciences at Microscale and Department of Physics, University of Science and Technology of China, Hefei, Anhui 230026, China

2.Key Laboratory of Strongly-coupled Quantum Matter Physics, University of Science and Technology of China, Chinese Academy of Sciences, Hefei, Anhui 230026, China

3. National Institute of Standards and Technology, Center for Neutron Research, 100 Bureau Dr., Gaithersburg, Maryland 20878, USA

4. Department of Physics, Renmin University of China, Beijing 100872, China

5.CAS Key Laboratory of Materials for Energy Conversion, Shanghai Institute of Ceramics, Chinese Academy of Sciences, Shanghai 200050, China

6. Beijing National Laboratory for Molecular Sciences and State Key Laboratory ofRare Earth Materials Chemistry and Applications, College of Chemistry and Molecular Engineering, Peking University, Beijing 100871, China

7. Department of Materials Science and Engineering, University of Maryland, College Park, Maryland 20742, USA

8. Collaborative Innovation Center of Advanced Microstructures, Nanjing 210093, China

DOI: 10.1038/NMAT4155

As is shown in Fig S1(a) and Fig S2(a), the Rietveld refinement usingX-ray powder diffraction data reveals the crystal structure is composed of alternating anti-PbOFeSe layer and anti-PbO type $LiFeO_2$ layer. The initial neutron powder diffraction indicated that there is no Li/Fe existing in this structure while only H-O connected with FeSe layer present in this compound as shown in Fig S1(b) and Fig S2(b).However, this structure proposed by NPD is extremely different from that determined byX-ray diffraction experiment. Therefore, the nuclear magnetic resonance was conducted to understand the different preliminary structural models suggested by X-ray and neutron diffraction experiments. NMR result definitely proved that both of Li and H should be contained in the same structure. After considering the NMR result with both Li and H in the structure, the final structure of $(Li_{0.8}Fe_{0.2})$OHFeSe is proposed and determined via Rietveld refinement of X-ray and neutron powder diffraction and NMR analysis. The $(Li_{0.8}Fe_{0.2})$OHFeSe structure and the corresponding Rietveld refinement pattern of NPD data are shown in Fig S1(c) and Fig S2(c), respectively. In this structure, FeSe layer is the conducting block, while $(Li_{0.8}Fe_{0.2})$OH layer is the charge reservoir block.

The refined structure parameters of $(Li_{0.8}Fe_{0.2})$OHFeSe from NPD data at different temperatures from 2.5K to 295K are summarized in Table S1. Selected bond distances and bond angles for the final $(Li_{0.8}Fe_{0.2})$OHFeSe structure model at different temperatures are also listed in Table S2.

The refined structure parameters of $(Li_{0.8}Fe_{0.2})$OHFeSe from NPD data with anisotropic temperature factors at 2.5K and 295K are summarized in Table S3.

In order to clarify the presence of OH in the (LiFe)OH layer instead of H_2O molecular, we conducted structural refinement to search for possible H_2O molecular with the NPD data collected at 4K.The schematic model and structure parameters are shown in Fig S3 and Table S4, respectively. The refinement shows strong anisotropic temperature factors in ab-plane, that is $U_{11}=U_{22}=4.3(1)$, $U_{33}=1.1(2)$, and occupancy is 1.04(1). Moreover, a model with splitting H to (0.7934(19), 0.7934(19), 0.1755(4)) from (0.75, 0.75, 0.1756(4)), and occupancy is 0.259(3). The result indicates that, at the H position, both of the models conclude that there is only one H atom at (0.75, 0.75, 0.1756) position which is the ideal position of H. Furthermore, the splitting model gives that the distances of H-H are smaller than 0.5 angstrom, and the angles of H-O-H are smaller than 30 degree, indicating impossible of presence of H_2O molecular. Thus, there is no possibility for the existence of disordered H_2O molecular at the OH position from NPD data.

Infrared reflectance spectroscopy measurement was also conducted on our sample to support the presence of purely OH and no H_2O molecule in the crystal structure. In order to get rid of the interference of H_2O in air, the experiment is conducted under high vacuum. The infrared reflectance spectroscopic data are shown in Fig S4. If there are H_2O molecules in the structure, the water bending mode would give a strong band around 1600 cm^{-1} in the infrared spectrum [1]. However, no anomaly can be observed around 1600 cm^{-1} in our infrared reflectance spectroscopy, which suggests that there is no H_2O molecule in the structure. Moreover, there exists a weak anomaly around 3600 cm^{-1} due to the OH-stretch mode [1-3], which is the evidence for the presence of OH in the structure. Therefore, Infrared reflectance spectroscopy definitely indicates that no H_2O molecule exists in this structure. In order to improve the quality of IR spectroscopy, the background is fitted using piecewise polynomial fit and then subtracted [4]. It can be seen clearly that a remarkable signal is observed around ~3600 cm^{-1} which arises from the OH-stretching mode. An asymmetric lineshape, which often appears in infrared reflectance spectroscopy experiment [5], is observed in the spectrum after subtracting background. It is well known that the signal of OH-bend mode is usually much weaker than the OH-stretching mode[6] and is usually absent in the IR experiment [2]. Due to the relatively weak signals attributed to the metallic properties of the compound, the OH-bend mode which might be expected to appear near 1000 cm^{-1} is too weak to be observed as shown in Fig.S4.

As is shown in Fig S5, the SEM photograph indicates the presence of plate-like single crystals with typical size of 20μm. Moreover, Energy Dispersive analysis of X-rays (EDX) is employed to determine the ratio of Fe and Se. In order to check the homogeneity of the sample, several spots were measured and the results were listed in the table. The results indicate that the chemical composition is homogeneous, and average atomic ratio of Fe:Se was determined to be 1.23(4):1 with an uncertainty ~3%.

Temperature-dependent electrical resistance measurement for the $(Li_{0.8}Fe_{0.2})$OHFeSe sample, which was pressed into pellet under high pressure, is shown in Figure S6. Since the as-grown sample is a powder product synthesized from the solution method as described in Method, the powder is just pressed into the pellet for the transport measurements. Therefore, the link between the grains is very weak and the grain boundaries contribute much to resistivity (especially below Tc), so thata very wide superconducting transition was observed, and the zero-resistance was reached at very low temperature (even cannot get zero-resistance). The

DOI: 10.1038/NMAT4155

resistivity data are not intrinsic and strongly dependent on how to press the powder into pellets (pressure and how dense), especially below Tc. As is shown in Figure S6, a very wide superconducting transition was observed below 40K and the zero-resistance was reached at 14K due to the contribution from grain boundaries. The drop of resistance starts at 40K which is consistent with the Tc determined from magnetic susceptibility.

Magnetization loops of the as-synthesized $(Li_{0.8}Fe_{0.2})$OHFeSe sample at 2 K, 5 K and 10 Kare shown in Figure S7. The M-H loop gradually becomes small with increasing the temperature, and especially the loop is closed under low filed at 10K above the magnetic ordering temperature. This is another evidence for magnetic order.

The thermoelectric power of the as-synthesized $(Li_{0.8}Fe_{0.2})$OHFeSe sample measured under magnetic field of 0T and 1T is shown in Figure S8. The absolute value of Seebeck coefficient for both 0T and 1T increase with decreasing temperature and reaches maximum of 57μV/K at ~138K. A rapid decrease in the absolute value of thermoelectric power takes place at 40K for 0T and at 39K for 1T, indicating the superconducting transition slightly shifts down to low temperature under 1 T.

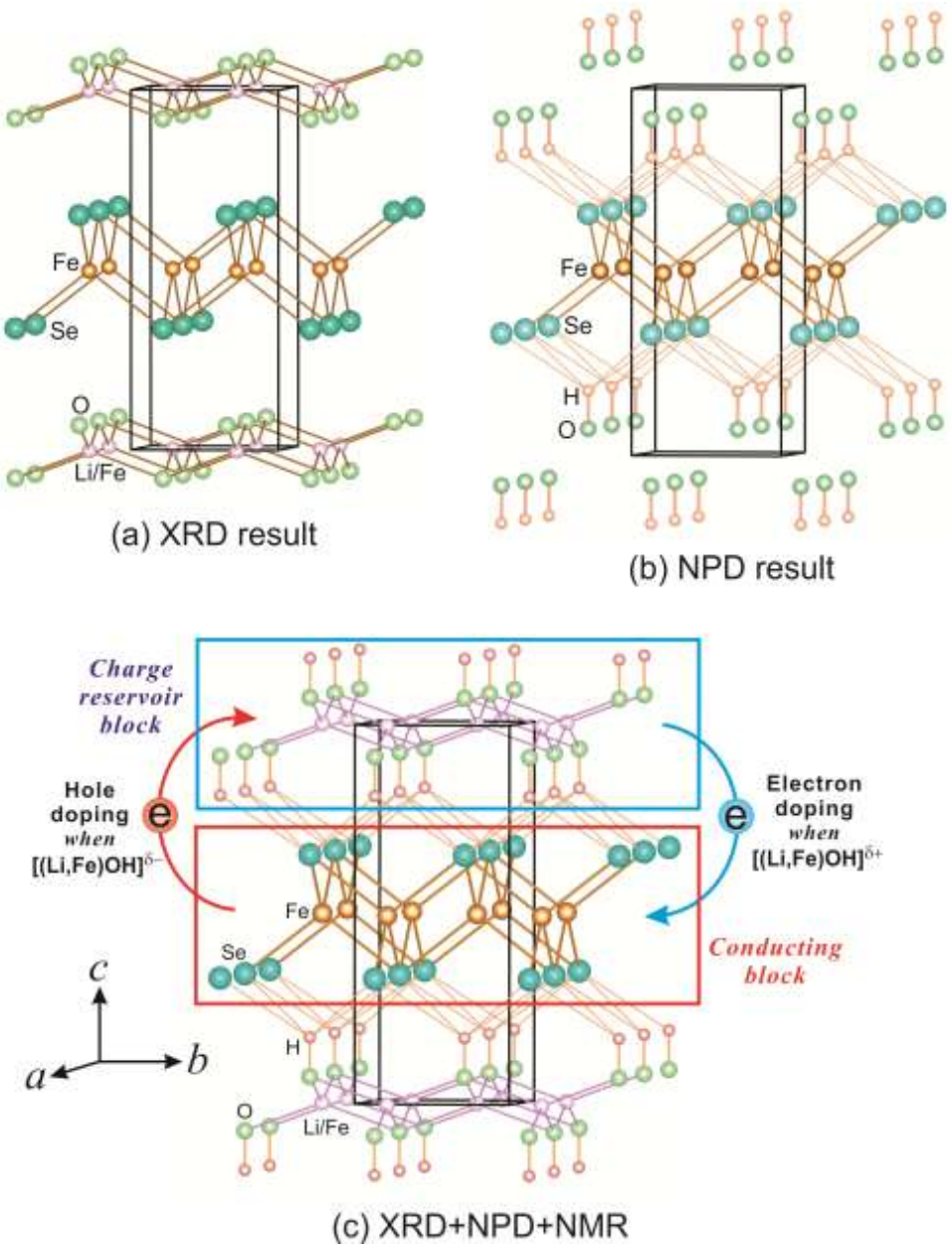

Figure S1. **(a):** Crystal structure of $LiFeO_2Fe_2Se_2$model, which was determinedfrom powder X-ray diffraction data. **(b):** A schematic structure of (OH)FeSe model from neutron powder diffraction data refinement result. In this model, OH layer and the FeSe layer are alternately stacked.**(c):** A schematic view of the structure of $(Li_{0.8}Fe_{0.2})$OHFeSe, which was determined by the combination of powder X-raydiffraction, neutron powder diffraction and nuclear magnetic resonance. The FeSe layer, which acts as the conducting block, alternately stacks with the charge reservoir block $(Li_{0.8}Fe_{0.2})$OH layer in this model.

DOI: 10.1038/NMAT4155

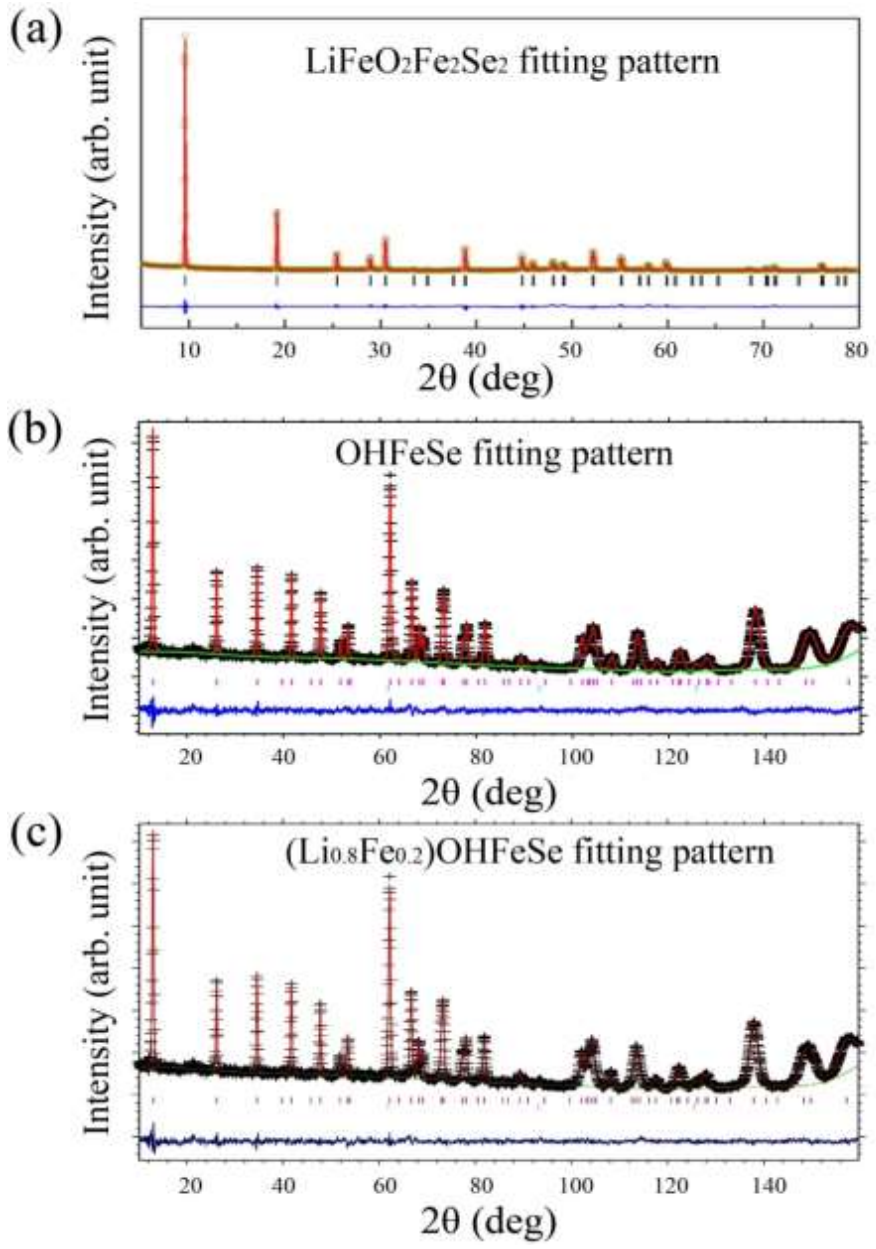

Figure S2: **(a):**Rietveld refinement onXRD data collected at 298K for the structural model of $LiFeO_2Fe_2Se_2$which was shown in Fig. S1(a).**(b):**Rietveld refinement on NPD data with the structural model of OHFeSeshown in Fig. S1(b). The NPD data wascollected over the 2-Theta range of 1.3-166.3° using Ge311(λ=2.0775Å) monochrometerat4K. **(c):**Rietveld refinementon NPD pattern which was collected at 4K using Ge311 (λ=2.0775Å) monochrometerwith the structural model of $(Li_{0.8}Fe_{0.2})$OHFeSeshown in Fig. S1(c).

Table S1: Structural parameters of $(Li_{0.8}Fe_{0.2})OHFeSe$from the NPD refinement for different temperature from 2.5K to 295K.

2.5K: *a*=3.77871(4) Å and c=9.1604(1) Å, Rwp=0.0183, Rp=0.015, χ^2=1.498

Atom	Wyckoff Site	x	y	z	Occup.	Uiso(x100 Å^2)
H	*2c*	0.75	0.75	0.1734(3)	1.00	2.79(8)
O	*2c*	0.25	0.25	-0.0764(1)	1.00	0.27(4)
Li	*2a*	0.75	0.25	0	0.81(1)	0.8 (fixed)
Fe1	*2a*	0.75	0.25	0	0.19(1)	0.8 (fixed)
Fe2	*2b*	0.75	0.25	0.5	1.00	0.52(2)
Se	*2c*	0.25	0.25	0.3390(1)	1.00	0.35(3)

4K: *a*=3.77887(6) Å and c=9.1609(2) Å, Rwp=0.0309, Rp=0.0251, χ^2=1.141

Atom	Wyckoff Site	x	y	z	Occup.	Uiso(x100 Å^2)
H	*2c*	0.75	0.75	0.1765(4)	1.00	3.08(8)
O	*2c*	0.25	0.25	-0.0759(2)	1.00	0.59(4)
Li	*2a*	0.75	0.25	0	0.81(1)	0.8 (fixed)
Fe1	*2a*	0.75	0.25	0	0.19(1)	0.8 (fixed)
Fe2	*2b*	0.75	0.25	0.5	1.00	0.55(2)
Se	*2c*	0.25	0.25	0.3386(1)	1.00	0.29(3)

15K: *a*=3.77947(7) Å and c=9.1617(3) Å, Rwp=0.0275, Rp=0.0223, χ^2=1.139

Atom	Wyckoff Site	x	y	z	Occup.	Uiso(x100 Å^2)
H	*2c*	0.75	0.75	0.1751(5)	1.00	3.3(1)
O	*2c*	0.25	0.25	-0.0748(2)	1.00	0.70(4)
Li	*2a*	0.75	0.25	0	0.80(1)	0.8 (fixed)
Fe1	*2a*	0.75	0.25	0	0.20(1)	0.8 (fixed)
Fe2	*2b*	0.75	0.25	0.5	1.00	0.46(4)
Se	*2c*	0.25	0.25	0.3369(2)	1.00	0.54(3)

295K: *a*=3.7860(1) Å and c=9.2880(9) Å, Rwp=0.0499, Rp=0.0412, χ^2=0.9065

Atom	Wyckoff Site	x	y	z	Occup.	Uiso(x100 Å^2)
H	*2c*	0.75	0.75	0.174(1)	1.00	5.0(2)
O	*2c*	0.25	0.25	-0.0737(6)	1.00	2.2(1)
Li	*2a*	0.75	0.25	0	0.82(1)	1.5 (fixed)
Fe1	*2a*	0.75	0.25	0	0.18(1)	1.5 (fixed)
Fe2	*2b*	0.75	0.25	0.5	1.00	1.57(5)
Se	*2c*	0.25	0.25	0.3384(5)	1.00	1.70(7)

DOI: 10.1038/NMAT4155

Table S2: Selected bond distance (Å) and bond angles (°)of $(Li_{0.8}Fe_{0.2})$OHFeSe for different temperature from 2.5K to 295K.

	2.5K	4K	15K	295K
Fe1/Li-O×4	2.0149(6)	2.0134(7)	2.0103(9)	2.013(2)
Fe2-Se ×4	2.4026(8)	2.3990(8)	2.4091(12)	2.416(3)
H-Se ×4	3.068(2)	3.057(2)	3.056(3)	3.078(7)
O-H	0.889(5)	0.922(5)	0.919(7)	0.94(2)
O-Li/Fe1-O ×2	139.3(1)	139.6(1)	140.1(1)	140.2(3)
×4	96.94(3)	96.85(3)	96.68(5)	96.7(1)
H-O-Li/Fe1 ×4	110.34(5)	110.21(5)	109.94(7)	109.9(2)
Se-Fe2-Se ×2	103.70(5)	103.92(5)	103.33(7)	103.2(2)
×4	112.43(3)	112.313)	112.63(4)	112.70(9)
O-H-Se ×4	119.43(6)	119.06(7)	119.01(9)	119.7(2)
Se-H-Se ×4	76.03(5)	76.35(6)	76.39(8)	75.9(2)
×2	121.2(1)	121.9(1)	122.0(2)	120.9(5)

Table S3:Structural parameters of $(Li_{0.8}Fe_{0.2})$OHFeSe from the NPD refinement with anisotropic temperature factors at 2.5K and 295K

2.5K: a=3.7781(2) Å and c=9.1586(3) Å, Rwp=0.0175, Rp=0.0144, χ^2=1.381

Atom	Wyckoff Site	x	y	z	Occup.	Uiso (x100Å^2)	U_{11} (x100Å^2)	U_{22} (x100Å^2)	U_{33} (x100Å^2)
H	*2c*	0.75	0.75	0.1755(2)	1.00		3.57(7)	3.57(7)	1.26(7)
O	*2c*	0.25	0.25	-0.0761(9)	1.00		0.60(8)	0.60(8)	0.17(8)
Li	*2a*	0.75	0.25	0	0.81(4)	0.800			
Fe1	*2a*	0.75	0.25	0	0.18(6)	0.800			
Fe2	*2b*	0.75	0.25	0.5	1.00		0.54(2)	0.54(2)	0.91(2)
Se	*2c*	0.25	0.25	0.3381(3)	1.00		0.53(6)	0.53(6)	0.53(2)

295K: a=3.7848(3) Å and c=9.2876(9) Å, Rwp=0.0478, Rp=0.0401, χ^2=0.8256

Atom	Wyckoff Site	x	y	z	Occup.	Uiso (x100Å^2)	U_{11} (x100Å^2)	U_{22} (x100Å^2)	U_{33} (x100Å^2)
H	*2c*	0.75	0.75	0.1765(2)	1.00		7.27(9)	7.27(9)	1.93(1)
O	*2c*	0.25	0.25	-0.0715(1)	1.00		1.98(4)	1.98(4)	2.17(5)
Li	*2a*	0.75	0.25	0	0.82(5)	2.000			
Fe1	*2a*	0.75	0.25	0	0.17(5)	2.000			
Fe2	*2b*	0.75	0.25	0.5	1.00		1.06(9)	1.06(9)	1.99(5)
Se	*2c*	0.25	0.25	0.3392(6)	1.00		1.23(6)	1.23(6)	1.86(7)

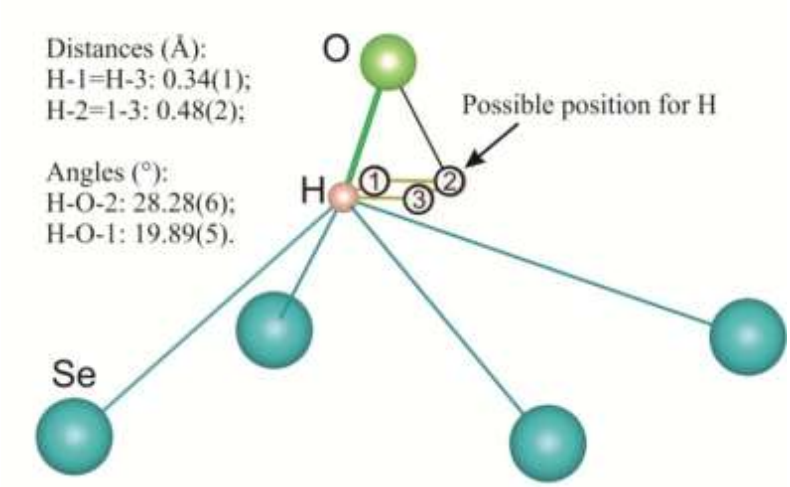

Figure S3. The schematic structure model of possible H_2O molecular in the structure

Table S4: The structure parameters of possible H_2O molecular which may presents at the OH using NPD data at 4K

Atom	*x*	*y*	*z*	Occup	Uiso (x100Å^2)	U_{11},U_{22} (x100Å^2)	U_{33} (x100 Å^2)
H	0.7934(19)	0.7934(19)	0.1755(4)	0.259(3)	1.1(1)		
	0.75	0.75	0.1756(4)	1.04(1)		4.3(1)	1.1(2)
O	0.25	0.25	-0.07607(2)	1.00	0.71(5)		
Li	0.75	0.25	0	0.814(2)	1		
Fe1	0.75	0.25	0	0.186(2)	1		
Fe2	0.75	0.25	0.5	1.00	0.68(3)		
Se	0.25	0.25	0.33898(1)	1.00	0.54(4)		

DOI: 10.1038/NMAT4155

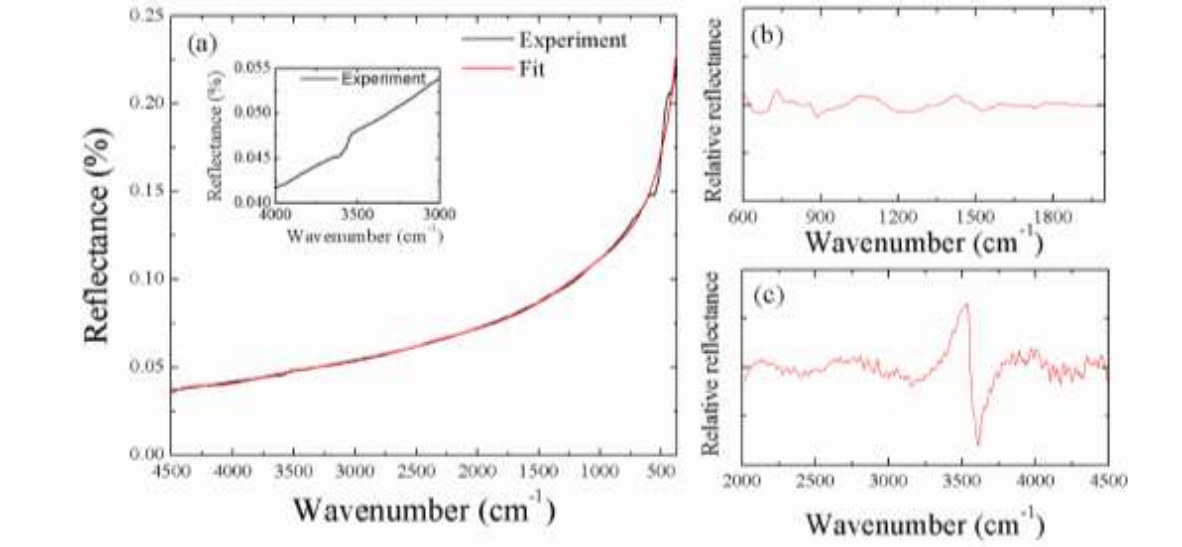

Figure S4. (a): The experiment IR reflectance spectroscopy and fitted background of $(Li_{0.8}Fe_{0.2})OHFeSe$; (b): The IR spectroscopy of 600-2000 cm^{-1} after subtracting the background; (c): The IR spectroscopy of 2000-4500 cm^{-1} after subtracting the background.

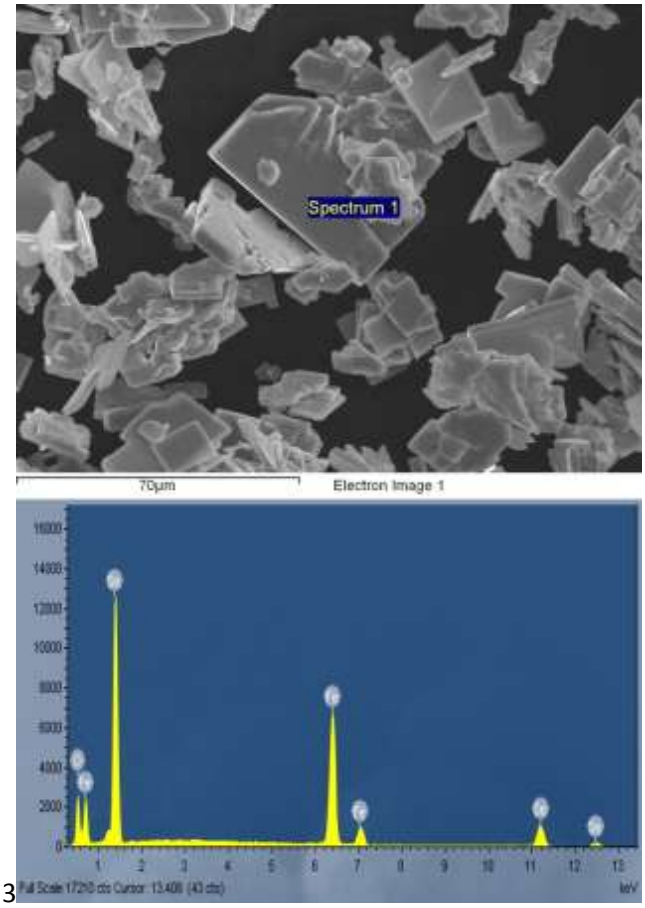

Point	Fe/Se (atomic)
1	1.19(4):1
2	1.25(4):1
3	1.25(4):1
4	1.18(4):1
5	1.26(4):1
Average	1.23(4):1

Figure S5. SEM micrograph and EDX analysis of $(Li_{0.8}Fe_{0.2})OHFeSe$ sample

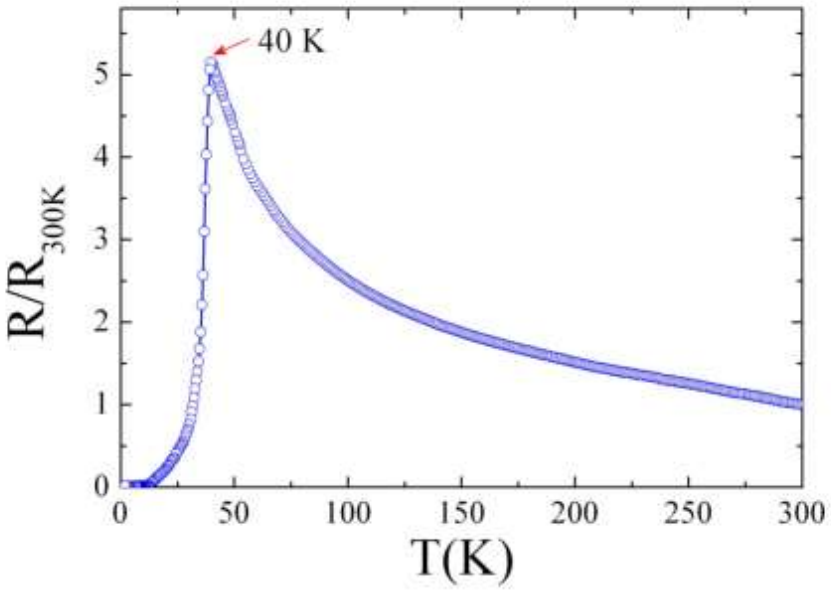

Figure S6. The temperature-dependent electrical resistance of the $(Li_{0.8}Fe_{0.2})OHFeSe$ sample.

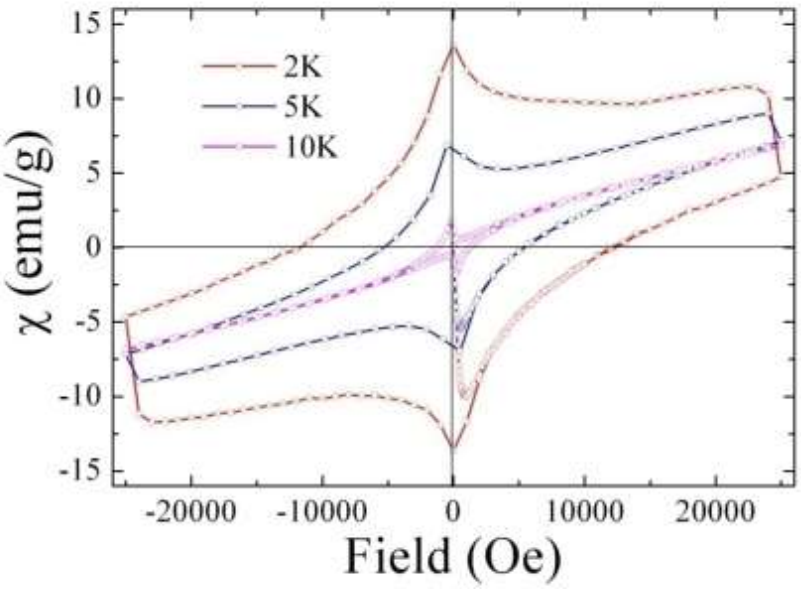

Figure S7. Magnetization loops of the as-synthesized $(Li_{0.8}Fe_{0.2})OHFeSe$ sample at T=2K, 5K, 10K, respectively.

DOI: 10.1038/NMAT4155

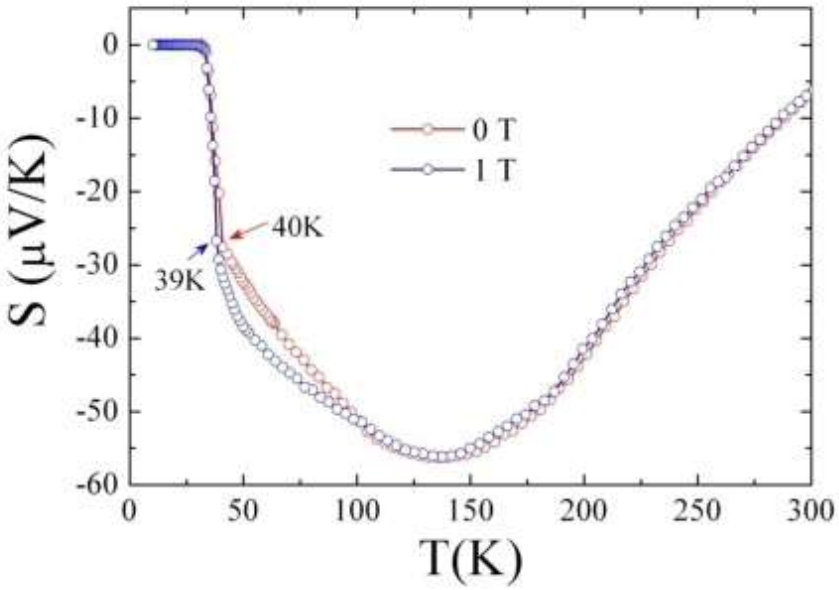

Figure S8. The thermoelectric power of the as-synthesized $(Li_{0.8}Fe_{0.2})OHFeSe$ sample measured under 0T and 1T magnetic field.

References

1. Parker, S. F. *et al.* Assignment of the vibrational spectra of lithium hydroxide monohydrate, $LiOH{\cdot}H_2O$. J. Chem. Phys. **134**, 084503 (2011)

2. Busing, W. R. *et al*. Infrared Spectra and Structure of NaOH and NaOD, J. Chem. Phys. **23**, 933 (1955)

3. Jones, L. H. *et al*. The Infrared Spectra and Structure of LiOH, $LiOH{\cdot}H_2O$ and the Deuterium Species. Remark on Fundamental Frequency of OH^-. J. Chem. Phys. **22**, 217 (1954)

4. Neubrech, F. et al. Plasmonic Enhancement of Vibrational Excitations in the Infrared. IEEE J. Sel. Top. Quant. Electron **19**, 4600809 (2013)

5. Miljković, M. *et al.*, Line shape distortion effects in infrared spectroscopy. Analyst **137**, 3954 (2012)

6. Smith, B. C. *Infrared Spectral Interpretation: A Systematic Approach* (CRC Press, Boca Raton, 1998)